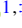


Controlling higher-orbital quantum phases of ultracold atoms via coupling to optical cavitiesHui Tan ^{1,*}, Jinsen Han ^{1,*}, Wei Zheng ^{2,3,4,†}, Jianmin Yuan,^{5,1} and Yongqiang Li ^{1,‡}¹*Department of Physics, National University of Defense Technology, Changsha 410073, People's Republic of China*²*Hefei National Laboratory for Physical Sciences at the Microscale and Department of Modern Physics, University of Science and Technology of China, Hefei 230026, People's Republic of China*³*CAS Center for Excellence in Quantum Information and Quantum Physics, University of Science and Technology of China, Hefei 230026, People's Republic of China*⁴*Hefei National Laboratory, University of Science and Technology of China, Hefei 230088, Peoples Republic of China*⁵*Department of Physics, Graduate School of China Academy of Engineering Physics, Beijing 100193, People's Republic of China*

(Received 15 July 2022; accepted 9 August 2022; published 24 August 2022)

The orbital degree of freedom plays an important role in understanding exotic phenomena of strongly correlated materials. In this work, we study strongly correlated ultracold bosonic gases coupled to a high-finesse cavity, pumped by a blue-detuned laser in the transverse direction. By controlling the reflection of the pump laser, we find that atoms can be selectively transferred to the odd-parity p -orbital band or to the even-parity d -orbital band of a two-dimensional square lattice, accompanied by pronounced cavity-photon excitations. By interacting with the cavity field, atoms self-organize to form stable higher-orbital superfluid and Mott-insulating phases with orbital-density waves, as a result of cavity-induced orbital-flip hoppings. Our study opens a route to manipulate orbital degrees of freedom in strongly correlated quantum gases via coupling to optical cavities.

DOI: [10.1103/PhysRevA.106.023315](https://doi.org/10.1103/PhysRevA.106.023315)**I. INTRODUCTION**

In condensed matter, electrons have three attributes: charge, spin, and orbital. Unlike charge and spin, the orbital exhibits strongly orientational properties and plays an important role in strongly correlated materials. For instance, highly anisotropic hoppings between different orbitals lead to a so-called orbital-selective Mott transition [1], and multiorbital-involved exotic pairings led to the debate about multiband superconductivity in heavy fermions [2]. From the aspect of quantum simulations, ultracold quantum gases provide a versatile platform for simulating charge and spin degrees of freedom to probe fundamental condensed-matter physics problems [3–7]. However, manipulating the orbital degree of freedom by using higher Bloch bands in optical lattices is not straightforward. On the one hand, fermionic atoms can populate higher-orbital bands by the Pauli principle, but that requires a high density of fermions [6]. On the other hand, bosonic atoms can be prepared in higher-orbital bands; however, they will decay into the lowest band due to collisions [8–10]. Recently, fascinating techniques have been proposed to study exotic orbital phenomena, including a shaking lattice [11,12] and a bipartite-lattice setup [13–17]. Observing the Fermi superfluid and strongly correlated Mott-insulating orbital order of ultracold gases, however, is still challenging [18–24].

Coupling ultracold atoms to a high-finesse optical cavity provides another tool for studying quantum many-body physics [25,26]. By choosing a pump-laser frequency that

is smaller than the atomic internal transition (red detuning), a self-organized superradiant phase has been theoretically predicted [27–35] and experimentally observed [36–43], where atoms break a translational symmetry by forming a density-wave pattern induced by cavity-mediated long-range interactions. For a quantum gas coupled to a blue-detuned cavity, self-organization of atoms should be prohibited since the buildup of additional repulsive potential costs energy. Surprisingly, a blue-detuned self-organized superradiant phase predicted recently [44–52] has already been observed experimentally [53,54]. It turns out that the blue-detuned cavity scatters atoms into higher-orbital bands, which triggers quantum engineering of many-body multiorbital physics with cavity setups. A remaining open question is to identify possibilities for simulating previously unrealized higher-orbital strongly correlated phenomena of ultracold atoms via coupling to optical cavities.

In this work, we present an experimentally related scheme to realize higher-orbital quantum phases of ultracold bosonic gases in an optical cavity, pumped by a blue-detuned laser. Within this setup, a considerable number of atoms can be stabilized in higher-orbital bands of the two-dimensional (2D) square lattice due to cavity-induced orbital-flipping processes, leading to previously untouched odd-parity p -orbital and even-parity d -orbital many-body phases. We find that the center-of-mass motion and orbital degree of freedom of atoms are coupled together, resulting in an “orbital-density-wave” order in both superfluid and Mott-insulating phases. In addition, we show that populations of atoms can be selectively tuned between the p - and d -orbital bands by controlling the reflection rate of the pump laser.

*These authors contributed equally to this work.

†zw8796@ustc.edu.cn

‡li_yq@nudt.edu.cn

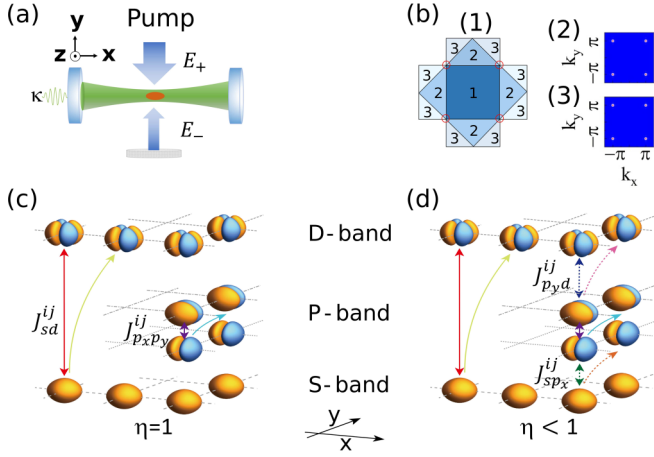


FIG. 1. Populating higher-orbital states with ultracold atoms in an optical cavity. (a) Atoms are prepared in an optical cavity, pumped by a blue-detuned laser in the transverse direction with an imbalance parameter $\eta = E_-/E_+$. (b) Brillouin zone of the square lattice, where atoms are scattered from the quasimomentum state $\mathbf{k} = (0, 0)$ to the excited state (π, π) , with quasimomentum distributions for the p - and d -orbital bands shown in plots 2 and 3, respectively. (c) and (d) Dominating scattering processes of atoms induced by the cavity, leading to higher-orbital excitations. By controlling η , atoms can be selectively scattered (c) into the even-parity d_{xy} -orbital state with a single node in both the x and y directions for $\eta = 1$ or (d) into the odd-parity p -orbital state with a single node only in one direction for $\eta < 1$. Here, J_{sd}^{ij} , $J_{p_x p_y}^{ij}$, $J_{s p_x}^{ij}$, and $J_{p_y d}^{ij}$ denote cavity-induced orbital-flip hoppings between sites i and j for the s and d_{xy} orbitals, p_x orbitals, s and p_x orbitals, and p_y and d_{xy} orbitals, respectively.

This paper is organized as follows: in Sec. II we introduce the setup and our approach. Section III covers the results of our model, and we derive the two-site model in Sec. IV. We briefly introduce the experimental detections in Sec. V and summarize with a discussion in Sec. VI.

II. MODEL AND METHOD

Our 2D setup is shown in Fig. 1(a), where ^{87}Rb atoms are loaded into a high-finesse single-mode optical cavity with a decay rate of $\kappa = 40\omega_r$, with ω_r being the recoil frequency. The two-level atoms with mass m and transition frequency ω_a (ground and excited states denoted by $|g\rangle$ and $|e\rangle$, respectively) are pumped by two counterpropagating blue-detuned lasers with wavelength $\lambda_p = 780.1$ nm and frequency ω_p in the y direction, perpendicular to the cavity mode with frequency ω_c in the x direction. The pump can be realized by applying one laser beam and reflection by a mirror, where the reflection rate controls the imbalance of the counterpropagating laser beams $\eta \equiv E_-/E_+$ [54], with E_+ and E_- being the electric-field amplitudes of the incident and reflected pump lasers, respectively. In the third direction, the motion of atoms is frozen with strong standing-wave lasers $V_z = 50E_r$, where $E_r = \frac{\hbar^2}{2m\lambda_p^2} = \hbar\omega_r$ is the recoil energy.

Assuming two unbalanced counterpropagating beams in the y direction, i.e., the incident light $E_+ \cos(k_p y - \omega_p t)$ and the reflected light $E_- \cos(k_p y + \omega_p t)$, the total electric field in

the y direction can be written as

$$\begin{aligned} E(y) &= E_0 \cos(k_p y - \omega_p t) + \eta E_0 \cos(k_p y + \omega_p t) \\ &= (1 + \eta) E_0 \cos(k_p y) \cos(\omega_p t) \\ &\quad + (1 - \eta) E_0 \sin(k_p y) \sin(\omega_p t), \end{aligned} \quad (1)$$

where $E_- = \eta E_+ = \eta E_0$ and k_p denotes the wave vector of the pumping field. Including the cavity mode in the x direction, the effective interaction between the atoms and total electric field of the system is described by

$$\begin{aligned} \hat{H}_{\text{int}} &= \hbar\Omega_p (1 + \eta) \cos(k_p y) (\hat{\sigma}^+ + \hat{\sigma}^-) \cos(\omega_p t) \\ &\quad + \hbar\Omega_p (1 - \eta) \sin(k_p y) (\hat{\sigma}^+ + \hat{\sigma}^-) \sin(\omega_p t) \\ &\quad + \hbar g_0 \cos(k_c x) (\hat{\sigma}^+ \hat{a} + \hat{\sigma}^- \hat{a}^\dagger), \end{aligned} \quad (2)$$

where $\hat{\sigma}^- = |g\rangle\langle e|$, $\hat{\sigma}^+ = |e\rangle\langle g|$, Ω_p denotes the maximum pump Rabi frequency, g_0 is the atom-cavity coupling strength, and \hat{a} (\hat{a}^\dagger) denotes the annihilation (creation) operator of a cavity photon with frequency ω_c . In the reference frame that rotates at the frequency ω_p , Eq. (2) can be written as

$$\begin{aligned} \hat{H}_{\text{int}} &= \frac{1}{2} \hbar\Omega_p (1 + \eta) \cos(k_p y) (\hat{\sigma}^+ + \hat{\sigma}^-) \\ &\quad + \frac{i}{2} \hbar\Omega_p (1 - \eta) \sin(k_p y) (\hat{\sigma}^+ - \hat{\sigma}^-) \\ &\quad + \hbar g_0 \cos(k_c x) (\hat{\sigma}^+ \hat{a} + \hat{\sigma}^- \hat{a}^\dagger). \end{aligned} \quad (3)$$

Taking the cavity mode and atom degrees of freedom into account, the many-body system can be described by

$$\begin{aligned} \hat{H} &= \int d\mathbf{x} \left[\hat{\Psi}_g^\dagger(\mathbf{x}) \left(-\frac{\hbar^2 \nabla^2}{2m} \right) \hat{\Psi}_g(\mathbf{x}) \right. \\ &\quad \left. + \hat{\Psi}_e^\dagger(\mathbf{x}) \left(-\frac{\hbar^2 \nabla^2}{2m} - \hbar\Delta_a \right) \hat{\Psi}_e(\mathbf{x}) \right] - \hbar\Delta_c \hat{a}^\dagger \hat{a} \\ &\quad + \int d\mathbf{x} \left[\hat{\Psi}_e^\dagger(\mathbf{x}) \left(\frac{\hbar\Omega_p (1 + \eta) \cos(k_p y)}{2} \right. \right. \\ &\quad \left. \left. + \frac{i\hbar\Omega_p (1 - \eta) \sin(k_p y)}{2} + \hbar g_0 \cos(k_c x) \hat{a} \right) \hat{\Psi}_g(\mathbf{x}) \right. \\ &\quad \left. + \text{H.c.} \right], \end{aligned} \quad (4)$$

where $\Delta_a = \omega_p - \omega_a$, $\Delta_c = \omega_p - \omega_c$, and $\hat{\Psi}_g(\mathbf{x})$ [$\hat{\Psi}_e(\mathbf{x})$] denotes the atomic field operator for annihilating an atom at position \mathbf{x} in the ground state (excited state).

Integrating out the excited state of the atom [55,56], the atomic system can be described by an effective Hamiltonian

$$\begin{aligned} \hat{H} &= \int d\mathbf{x} \hat{\Psi}^\dagger(\mathbf{x}) \left(-\frac{\hbar^2}{2m} \nabla^2 + \eta V_p \cos^2(k_p y) \right. \\ &\quad \left. + U_0 \cos^2(k_c x) \hat{a}^\dagger \hat{a} + \hat{V}_{1,\text{scat}} + \hat{V}_{2,\text{scat}} \right) \hat{\Psi}(\mathbf{x}) \\ &\quad + \frac{g}{2} \int d\mathbf{x} \hat{\Psi}^\dagger(\mathbf{x}) \hat{\Psi}^\dagger(\mathbf{x}) \hat{\Psi}(\mathbf{x}) \hat{\Psi}(\mathbf{x}) - \hbar\Delta_c \hat{a}^\dagger \hat{a}. \end{aligned} \quad (5)$$

$\hat{\Psi}(\mathbf{x})$ denotes the atomic field operator for the ground state, where the excited state has been adiabatically eliminated due to the negligible spontaneous emission for very

low temperature and large detuning Δ_c . $V_p = \hbar\Omega_p^2/\Delta_a$ is the depth of the standing-wave potential created by the pump laser in the y direction, and $U_0 = \hbar g_0^2/\Delta_a$ is the light shift of a single maximally coupled atom. Here, we choose the wave vectors of the pumping and cavity fields to be identical, with $k_c = k_p$. The dominant term is the interference between the pumping and cavity fields with $\hat{V}_{1,\text{scat}} = \frac{(1+\eta)}{2}\sqrt{V_p U_0}(\hat{a} + \hat{a}^\dagger)\cos(k_c x)\cos(k_p y)$ and $\hat{V}_{2,\text{scat}} = -i\frac{(1-\eta)}{2}\sqrt{V_p U_0}(\hat{a} - \hat{a}^\dagger)\cos(k_c x)\sin(k_p y)$. We remark here that contact interactions $g = \frac{4\pi\hbar^2 a_s}{m}$ between atoms have been added in the many-body Hamiltonian, with a_s being the s -wave scattering length.

Actually, for a blue-detuned pump laser, atoms localize in the minima of the potential, which is shifted by $\lambda/4$ in both the cavity and pump directions, compared to the red-detuned case. Thus, we treat the position of the atoms as the origin of the coordinate system, and the effective Hamiltonian can be written as

$$\begin{aligned} \hat{H} = & \int d\mathbf{x} \hat{\Psi}^\dagger(\mathbf{x}) \left(-\frac{\hbar^2}{2m} \nabla^2 + \eta V_p \sin^2(k_p y) \right. \\ & \left. + U_0 \sin^2(k_c x) \hat{a}^\dagger \hat{a} + \hat{V}_{1,\text{scat}} + \hat{V}_{2,\text{scat}} \right) \hat{\Psi}(\mathbf{x}) \\ & + \frac{g}{2} \int d\mathbf{x} \hat{\Psi}^\dagger(\mathbf{x}) \hat{\Psi}^\dagger(\mathbf{x}) \hat{\Psi}(\mathbf{x}) \hat{\Psi}(\mathbf{x}) - \hbar\Delta_c \hat{a}^\dagger \hat{a}, \quad (6) \end{aligned}$$

with $\hat{V}_{1,\text{scat}} = \frac{(1+\eta)}{2}\sqrt{V_p U_0}(\hat{a} + \hat{a}^\dagger)\sin(k_c x)\sin(k_p y)$ and $\hat{V}_{2,\text{scat}} = i\frac{(1-\eta)}{2}\sqrt{V_p U_0}(\hat{a} - \hat{a}^\dagger)\sin(k_c x)\cos(k_p y)$.

In a sufficiently deep lattice, we can use the tight-binding approximation and keep finite relevant bands, such that the system can be described by a generalized Bose-Hubbard model (see Sec. A 1),

$$\begin{aligned} \hat{H} = & - \sum_{\langle ij \rangle, \sigma} J_{\sigma\sigma}^{ij} \hat{b}_{i,\sigma}^\dagger \hat{b}_{j,\sigma} - \sum_{i,\sigma} \mu_\sigma \hat{b}_{i,\sigma}^\dagger \hat{b}_{i,\sigma} - \hbar\Delta_c \hat{a}^\dagger \hat{a} \\ & + \sum_{i,\sigma_1\sigma_2\sigma_3\sigma_4} \frac{U_{\sigma_1\sigma_2\sigma_3\sigma_4}}{2} \hat{b}_{i,\sigma_1}^\dagger \hat{b}_{i,\sigma_2}^\dagger \hat{b}_{i,\sigma_3} \hat{b}_{i,\sigma_4} + \hat{V}_1 + \hat{V}_2, \quad (7) \end{aligned}$$

where $\hat{V}_1 = (\hat{a} + \hat{a}^\dagger) \sum_{ij} (-1)^j (J_{sd}^{ij} \hat{b}_{i,s}^\dagger \hat{b}_{j,d} + J_{p_x p_y}^{ij} \hat{b}_{i,p_x}^\dagger \hat{b}_{j,p_y} + \text{H.c.})$ and $\hat{V}_2 = -i(\hat{a} - \hat{a}^\dagger) \sum_{ij} (-1)^j (J_{s p_x}^{ij} \hat{b}_{i,s}^\dagger \hat{b}_{j,p_x} + J_{p_y d}^{ij} \hat{b}_{i,p_y}^\dagger \hat{b}_{j,d} + \text{H.c.})$ are the cavity-induced scattering processes, $\langle i, j \rangle$ denotes the nearest-neighbor sites, $J_{\sigma_1\sigma_2}^{ij}$ are the on-site ($i = j$) and nearest-neighbor ($i \neq j$) single-particle hopping amplitudes, $\mu_\sigma \equiv J_{\sigma\sigma}^{ii}$ is the chemical potential, and $U_{\sigma_1\sigma_2\sigma_3\sigma_4}$ is the on-site interactions. $\hat{b}_{i,\sigma}$ denotes the annihilation operator for the Wannier state σ at site i , with σ denoting the s orbital and p_x and p_y orbitals with a single node only in one direction and the d_{xy} orbital with a single node in both directions. All the Hubbard parameters are obtained from band-structure calculations of the 2D square lattice (see Sec. A 1). To validate the tight-binding model, an external optical lattice is added in the cavity direction, which has been set to $5E_r$ in our simulations.

Generally, the dominating process is the cavity-induced scattering of atoms, where the parity of the scattering and dimension of the system play important roles. Atoms are dominantly scattered to the s -orbital band for the red atom-pump

detuning due to the even parity of the scattering [36] and excited to higher-orbital bands for the blue-detuned case, as a result of the odd parity of the scattering [53]. In the 2D blue-detuned system considered here, we notice that atoms can populate in odd-parity p -orbital and even-parity d -orbital bands, stabilizing strongly correlated higher-orbital phases. As shown in Fig. 1(c), \hat{V}_1 scatters the atoms from the s to d_{xy} orbital and from the p_x to p_y orbital since \hat{V}_1 is parity odd in both the x and y directions, which changes the parity of orbitals in both the x and y directions. \hat{V}_2 scatters the atoms from the s to p_x orbital and from the p_y to d_{xy} orbital since \hat{V}_2 is parity odd in the x direction but even in the y direction, which changes the parity of the orbitals only in the x direction, as shown in Fig. 1(d). In addition, due to the factor $(-1)^i$, we note that the interference terms \hat{V}_1 and \hat{V}_2 will transfer a quasimomentum by (π, π) at the same time as they flip the orbitals, as shown in Fig. 1(b).

In the superradiant phase, the cavity mode is macroscopically populated, such that the cavity field can be approximated by its mean value $\alpha(t) = \langle \hat{a}(t) \rangle$ [57]. In the steady state, $\partial_t \alpha(t) = 0$, the cavity field is determined self-consistently with

$$\begin{aligned} \alpha = & \sum_i (-1)^i \langle J_{sd}^{ii} \hat{b}_{i,s}^\dagger \hat{b}_{i,d} + J_{p_x p_y}^{ii} \hat{b}_{i,p_x}^\dagger \hat{b}_{i,p_y} + \text{H.c.} \\ & + i(J_{s p_x}^{ii} \hat{b}_{i,s}^\dagger \hat{b}_{i,p_x} + J_{p_y d}^{ii} \hat{b}_{i,p_y}^\dagger \hat{b}_{i,d} + \text{H.c.}) \rangle / \\ & \left(\Delta_c - \sum_{i,\sigma} \langle J_\sigma \hat{b}_{i,\sigma}^\dagger \hat{b}_{i,\sigma} \rangle + i\kappa \right), \end{aligned}$$

where J_σ denotes the on-site matrix elements associated with the cavity (see Sec. A 1). In the following, we will mainly focus on the many-body phases of the atoms in the superradiant regime of the cavity. To obtain the steady state of the many-body system, we numerically solve Eq. (7) in the coherent-state approximation for the cavity mode by using real-space bosonic dynamical mean-field theory, which provides a nonperturbative description of many-body systems both in three and two dimensions [58–61], whose reliability has been compared against quantum Monte Carlo simulations [62]. Recently, a four-component bosonic dynamical mean-field theory was developed to study multispecies bosons in the p -orbital band [63]. Here, we implement this method to tackle the multiband system, and the technical details are described in Sec. A 2.

III. RESULTS

A. d -orbital population for a perfect reflection

We first discuss the physics for a perfect reflection of the pump laser, $\eta = 1$. To characterize the many-body phases, the mean cavity-photon number $|\alpha|^2$, superfluid order parameter $\phi_\sigma = \sum_i |\langle \hat{b}_{i,\sigma} \rangle| / N_{\text{lat}}$, and orbital magnetism $\hat{S}_{i,\sigma_2\sigma_1}^{\sigma_2\sigma_1} = \hat{b}_{i,\sigma_2}^\dagger \mathbf{F}_{\sigma_2\sigma_1} \hat{b}_{i,\sigma_1}$ are utilized, where N_{lat} denotes the total number of lattice sites and $\mathbf{F}_{\sigma_2\sigma_1}$ is the Pauli matrices for spin 1/2. Since the pump laser globally couples to all atoms in the cavity, the atom number in turn shifts the phase boundary. This motivates us to fix the rescaled atom-cavity coupling $N_{\text{lat}} \times U_0$ in our simulations.

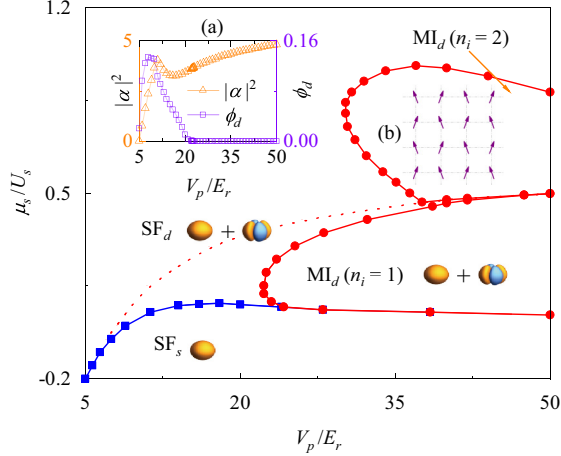


FIG. 2. Phase diagram of bosonic gases trapped in an optical cavity, pumped by a blue-detuned laser with the imbalance parameter $\eta = 1$, obtained from bosonic dynamical mean-field theory. There are three many-body phases, including the s -orbital superfluid phase (SF_s) without superradiance and d -orbital superfluid (SF_d) and Mott-insulating (MI_d) phases with superradiance of the cavity field. Insets: (a) Photon number $|\alpha|^2$ and d -orbital order parameter ϕ_d as a function of the pump laser depth for a fixed chemical potential $\mu_s/U_s = 0.15$, with U_s being on-site interactions between atoms in the s -orbital band, indicating a d -orbital superfluid-Mott-insulating phase transition, and (b) real-space distribution of orbital order $\langle \hat{S}_{x,z}^{sd} \rangle$ for the d -orbital phases with $\langle \hat{S}_y^{sd} \rangle = 0$. Other parameters are $N_{\text{lat}} \times U_0 = 600E_r$, $\Delta_c = 80\omega_r$, and $\kappa = 40\omega_r$, with N_{lat} being the total number of lattice sites and U_0 being the light shift per photon.

In contrast to the red-detuned case [34], we observe that a few percent of the atoms are transferred from the s - to d_{xy} -orbital band with considerable cavity-photon excitations [Fig. 2, inset (a)] by a blue-detuned pump laser, stabilizing the d -orbital superfluid and Mott-insulating phases. As shown in Figs. 2 and 3, three quantum phases appear, including the

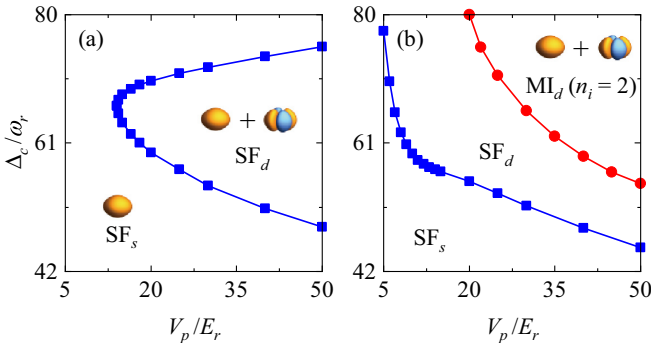


FIG. 3. Phase diagram of bosonic gases pumped by a blue-detuned laser with the imbalance parameter $\eta = 1$ as a function of cavity detuning Δ_c and pump lattice depth V_p , obtained from bosonic dynamical mean-field theory. (a) For the weak atom-cavity coupling $N_{\text{lat}} \times U_0 = 240E_r$, there exist s -orbital superfluid (SF_s) and d -orbital superfluid (SF_d) phases, and (b) for the strong coupling $N_{\text{lat}} \times U_0 = 400E_r$, there exist s -orbital superfluid (SF_s), d -orbital superfluid (SF_d), and Mott-insulating (MI_d) phases. Here, the local total filling $n_i = 2$, and the decay rate $\kappa = 40\omega_r$.

s -orbital superfluid phase (SF_s) with $|\alpha|^2 = 0$, the d -orbital superfluid phase (SF_d) with $|\alpha|^2 \neq 0$ and $\phi_d \neq 0$, and the d -orbital Mott-insulating phase (MI_d) with $|\alpha|^2 \neq 0$ and $\phi_s = \phi_d = 0$. As a result of the symmetry of p -orbital states, we observe only the neglected p -orbital population, induced by on-site interactions [19,20,64–67]. We remark here that including even more higher-orbital states will induce additional complications for our theoretical analysis but is not expected to affect our results qualitatively as a result of the large band gap in the deep lattices.

A filling-dependent phase diagram is shown in Fig. 2 as a function of the chemical potential and pumping strength. For a smaller chemical potential μ_s , the coupling between the atoms and cavity mode is so weak that the photon number in the cavity mode $|\alpha|^2 = 0$, with only the s -orbital band being populated. By increasing the chemical potential, the d -orbital superfluid phase appears since the scattering is a collective effect due to all the atoms in the cavity and depends on the total particle number. For a stronger pumping strength, more photons are scattered into the cavity mode, and the resulting standing wave in the cavity direction suppresses the tunneling of atoms in the absence of superfluidity $\phi_s = \phi_d = 0$. As shown in inset (a) in Fig. 2, we clearly observe the d -orbital superfluid-Mott-insulating phase transition upon increasing the depth of the pump laser. Note here that the dotted red line corresponds to the maximum values of $|\alpha|^2$ for fixed μ_s/U_s . This line is due to the characteristics of the Bose-Hubbard model. On the one hand, with the increase of the pump laser strength, more photons are scattered into the cavity mode, but on the other, the decrease in the atoms number weakens the collective scattering effect, leading to a maximum value of $|\alpha|^2$. Finally, the d -orbital Mott-insulating phase appears, which yields a fixed atom number and stabilizes the superradiant phase. We note that by tuning the light shift $L \times U_0$, a Mott-insulator phase with different filling can be achieved (see Sec. A 3).

Because they are relevant to the experiments, we also map out phase diagrams as a function of cavity detuning Δ_c and pump lattice depth V_p for a fixed filling $n_i = \sum_{\sigma} \langle \hat{b}_{i,\sigma}^\dagger \hat{b}_{i,\sigma} \rangle = 2$, with $N_{\text{lat}} \times U_0 = 240E_r$ [Fig. 3(a)] and $N_{\text{lat}} \times U_0 = 400E_r$ [Fig. 3(b)]. Three different phases exist for the parameters studied here, including the SF_s , SF_d , and MI_d phases, where the d -orbital phases occupy a large part of the phase diagrams, indicating large opportunities for experimental observation. As expected, both SF_d and MI_d phases appear for a stronger coupling between the atoms and cavity mode, as shown in Fig. 3(b). On the other hand, only the SF_d phase appears for a weaker atom-cavity coupling, as shown in Fig. 3(a).

B. P -orbital population for an imperfect reflection

In this part, we discuss an imperfect reflection of the pump laser, $\eta < 1$. Here, $\hat{V}_2 \neq 0$ scatters atoms to the p -orbital band. This process competes with the \hat{V}_1 term, which excites atoms to the d -orbital band. Therefore, both p - and d -orbital degrees of freedom come into play, indicating even richer physics, as shown in Fig. 4.

We observe four stable phases, including the SF_s , SF_d , $(p+d)$ -orbital superfluid (SF_{p+d}), and $(p+d)$ -orbital Mott-insulating (MI_{p+d}) phases. As expected, the system is an

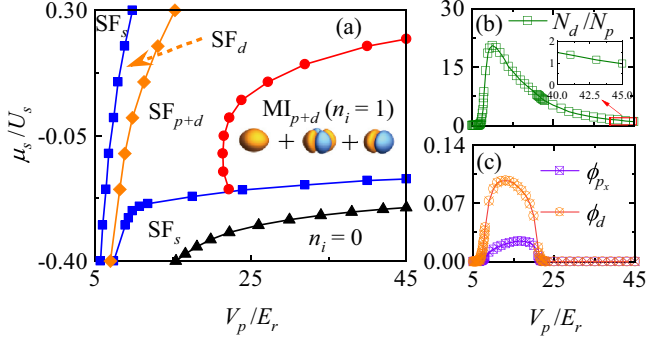


FIG. 4. Phase diagram of ultracold bosonic gases trapped in an optical cavity, pumped by a blue-detuned laser with an imbalance parameter $\eta = 0.8$, obtained from bosonic dynamical mean-field theory. (a) In addition to the d -orbital populated phase (SF_d), we observe superposition of the p_x - and d_{xy} -orbital atoms in the self-organized superfluid (SF_{p+d}) and Mott-insulating (MI_{p+d}) phases. (b) The ratio of total atom numbers of the p - and d -orbital bands and (c) superfluid order parameters ϕ_{p_x} and ϕ_d are shown as a function of the pump laser depth for a fixed chemical potential $\mu_s/U_s = 0$. The inset in (b) is a zoom of the main figure for a stronger pump strength. Other parameters are $\Delta_c = 100\omega_r$, $\kappa = 40\omega_r$, and $N_{\text{lat}} \times U_0 = 1200E_r$.

s -orbital superfluid phase in the absence of cavity photons for a smaller pumping strength. With the increase of the pumping power V_p , more photons are scattered into the cavity, and atoms organize themselves by being first excited to the d_{xy} -orbital band, stabilizing the SF_d phase. Upon further increasing pumping power, the p -orbital band is also populated, and the system enters a new superfluid phase, SF_{p+d} , with both p_x - and d_{xy} -orbital states being populated. Finally, in the strong pumping limit, the system enters the Mott-insulating phase, MI_{p+d} , with atoms localized in a superposition of local p_x and d_{xy} orbitals. Note here that only a tiny fraction of the atoms populates in the p_y -orbital state since scattering atoms to the p_y orbital is a higher-order process, as shown in Fig. 1(d).

To characterize the transition between these phases, population ratios in different bands N_d/N_p and superfluid order parameters are utilized, as shown in Figs. 4(b) and 4(c), where $N_\sigma = \sum_i \langle \hat{b}_{i,\sigma}^\dagger \hat{b}_{i,\sigma} \rangle$. We observe that the population in the d -orbital band increases quickly with the pumping strength. However, the population of the p -orbital is tiny for a shallow lattice, indicating the d -orbital phase appears first. When the pumping strength exceeds a critical value, the p -orbital band starts to become populated, eventually being the same order as the d orbital, as shown in the inset of Fig. 4(b). Finally, the atoms are localized in the absence of superfluid order parameters $\phi_\sigma = 0$, indicating the appearance of a Mott-insulating phase, as shown in Fig. 4(c).

We remark here that the population of higher-orbital states can be tuned by the imbalance η . When $\eta \sim 1$, V_1 dominates the scattering processes by transferring atoms into the d -orbital band, and we do observe a pronounced d -orbital population with negligible p -orbital excitations (Figs. 2 and 3). For smaller η , V_2 dominates the scattering processes by exciting atoms into the p -orbital band due to the relatively small band gap between the s - and p -orbital bands. For $\eta = 0.6$, we find that 20% of atoms populate in the p -orbital band but with negligible population in the d -orbital band, as shown in

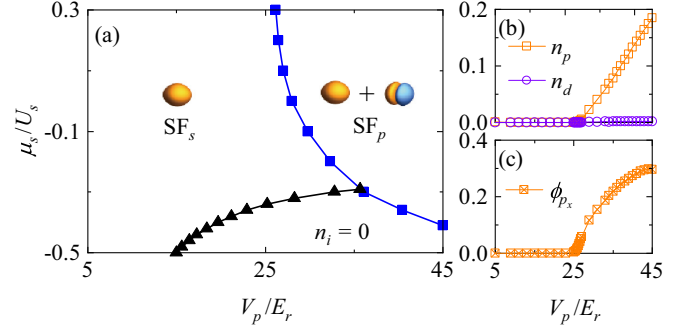


FIG. 5. (a) Phase diagram of ultracold bosonic gases trapped in an optical cavity, pumped by a blue-detuned laser with an imperfect reflection $\eta = 0.6$. (b) The average population of the atoms in the p -orbital states $n_p = \sum_i (n_{i,p_x} + n_{i,p_y})/N_{\text{lat}}$ and the d -orbital state $n_d = \sum_i n_{i,d}/N_{\text{lat}}$ and (c) the order parameter ϕ_{p_x} are shown as a function of the pump laser depth along the line $\mu_s = 0.3U_s$, indicating the scattering processes involved dominant p -orbital states. The other parameters are $N_{\text{lat}} \times U_0 = 1200E_r$ and $\Delta_c = -20\omega_r$.

Fig. 5(b), where a new phase, the p -orbital superfluid phase (SF_p), is found, defined as $|\alpha|^2 \neq 0$ and $\phi_p \neq 0$. As shown in Fig. 5(a), there are two many-body phases, including the s -orbital superfluid phase (SF_s) in the absence of photons in the cavity and the p -orbital superfluid phase (SF_p) in the presence of photons in the cavity. Our numerical results thus confirm the possibility for selectively preparing atoms in different higher-orbital bands in an optical cavity system.

IV. ORBITAL-DENSITY WAVE IN THE MOTT-INSULATING REGIME

In this part, we discuss the underlying physics of the self-organized phases, especially in the strongly correlated Mott regime. Distinct from the emergent superradiant phases with charge-density waves for a red-detuned cavity, the excited atoms appear with self-organized orbital-density waves for the blue-detuned case due to cavity-induced orbital-flip hoppings, as shown in Fig. 2(b), where the local total filling is homogeneous.

To characterize the many-body phenomena, orbital degrees of freedom are mapped to pseudospins. For example, one treats the s -orbital atoms as spin \uparrow and the d -orbital and p -orbital atoms as spin \downarrow and essentially achieves a pseudospin-1/2 system in optical lattices. Here, local magnetism of the system is given by $\hat{S}^{\sigma_1\sigma_2}$, i.e., $\hat{S}_x^{sd} = 1/2(\hat{b}_{i,s}^\dagger \hat{b}_{i,d} + \hat{b}_{i,d}^\dagger \hat{b}_{i,s})$, $\hat{S}_y^{sd} = i/2(-\hat{b}_{i,s}^\dagger \hat{b}_{i,d} + \hat{b}_{i,d}^\dagger \hat{b}_{i,s})$, and $\hat{S}_z^{sd} = 1/2(\hat{b}_{i,s}^\dagger \hat{b}_{i,s} - \hat{b}_{i,d}^\dagger \hat{b}_{i,d})$ for the s - and d -orbital degrees of freedom. Similarly, $\hat{S}_x^{sp_x} = 1/2(\hat{b}_{i,s}^\dagger \hat{b}_{i,p_x} + \hat{b}_{i,p_x}^\dagger \hat{b}_{i,s})$, $\hat{S}_y^{sp_x} = i/2(-\hat{b}_{i,s}^\dagger \hat{b}_{i,p_x} + \hat{b}_{i,p_x}^\dagger \hat{b}_{i,s})$, and $\hat{S}_z^{sp_x} = 1/2(\hat{b}_{i,s}^\dagger \hat{b}_{i,s} - \hat{b}_{i,p_x}^\dagger \hat{b}_{i,p_x})$ for the s - and p_x -orbital degrees of freedom.

A. Orbital-density-wave order for filling $n_i = 1$ and reflection $\eta = 1$

For a perfect reflection of the blue-detuned pump laser with $\eta = 1$, the atoms are transferred from the s - to d -orbital state with negligible populations in the p -orbital band. Therefore, we eliminate the terms related to p -orbital degrees of freedom

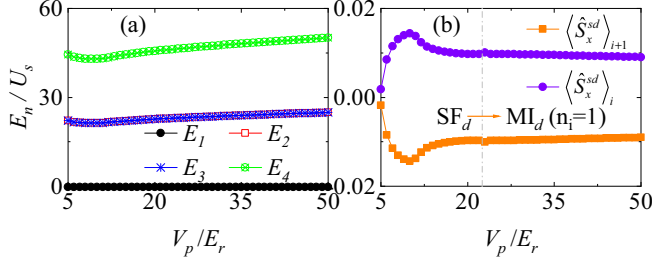


FIG. 6. (a) Eigenvalues E_n of the two-site model for perfect reflection $\eta = 1$. (b) Long-range orders of the ground state $|g_1\rangle$ with $n_i = 1$, calculated by using the parameters obtained via band-structure simulations. The other parameters are $N_{\text{lat}} \times U_0 = 600E_r$, $\Delta_c = 80\omega_r$, $\kappa = 40\omega_r$, and $\mu_s/U_s = 0.15$.

and rewrite Eq. (7) in the zero-hopping limit,

$$\begin{aligned} \hat{H}_0 = & 2\text{Re}[\alpha] \sum_i (-1)^i J_{sd}^{ii} (\hat{b}_{i,s}^\dagger \hat{b}_{i,d} + \text{H.c.}) \\ & + \frac{U_s}{2} \sum_i \hat{n}_{i,s} (\hat{n}_{i,s} - 1) + \frac{U_d}{2} \sum_i \hat{n}_{i,d} (\hat{n}_{i,d} - 1) \\ & + 2U_{sd} \hat{n}_{i,s} \hat{n}_{i,d} + \frac{U_{sd}}{2} (\hat{b}_{i,s}^\dagger \hat{b}_{i,s}^\dagger \hat{b}_{i,d} \hat{b}_{i,d} + \text{H.c.}) \\ & - \sum_{i,\sigma} \mu_\sigma \hat{b}_{i,\sigma}^\dagger \hat{b}_{i,\sigma}, \end{aligned}$$

where it includes the on-site interactions, scattering terms, and chemical potential.

In the deep Mott-insulating phase with local total filling $n_i = 1$, the two-site Hamiltonian for sites i and $i + 1$ can be written in matrix form under the basis of $|s, s\rangle$, $|s, d\rangle$, $|d, s\rangle$, $|d, d\rangle$,

$$H_0 = \begin{pmatrix} -2\mu_s & -J_1 & J_1 & 0 \\ -J_1 & -\mu_s - \mu_d & 0 & J_1 \\ J_1 & 0 & -\mu_s - \mu_d & -J_1 \\ 0 & J_1 & -J_1 & -2\mu_d \end{pmatrix}, \quad (8)$$

where $J_1 = 2\text{Re}[\alpha] J_{sd}^{ii}$ and the states $|\sigma, \sigma'\rangle = \hat{b}_{i,\sigma}^\dagger \hat{b}_{i+1,\sigma'}^\dagger |0, 0\rangle$. All the parameters are obtained from band-structure simulations.

After diagonalizing the Hamiltonian H_0 , we obtain the eigenstates

$$\begin{aligned} |g_n\rangle = & \sum_{\sigma,\sigma'} A_{n,\sigma,\sigma'} |\sigma, \sigma'\rangle \\ = & A_{n,s,s} |s, s\rangle + A_{n,s,d} |s, d\rangle + A_{n,d,s} |d, s\rangle \\ & + A_{n,d,d} |d, d\rangle, \end{aligned}$$

with energies E_n for $n = 1, 2, 3, 4$. Figure 6(a) shows the eigenenergies as a function of the pump strength, where the degeneracy of the ground states is broken due to the large on-site scattering J_1 and the difference in the chemical potential between the s and d orbitals. Thus, under the ground state $|g_1\rangle$ in Mott-insulating phase, the corresponding orbital-density wave order is $\langle \hat{S}_x^{sd} \rangle_i = -\langle \hat{S}_x^{sd} \rangle_{i+1}$, as shown in Fig. 6(b), where $\langle \cdots \rangle_i$ denotes the average value for site i . Note here that the higher-order perturbations as a result of nearest-neighbor hopping and scattering terms can be neglected, which slightly

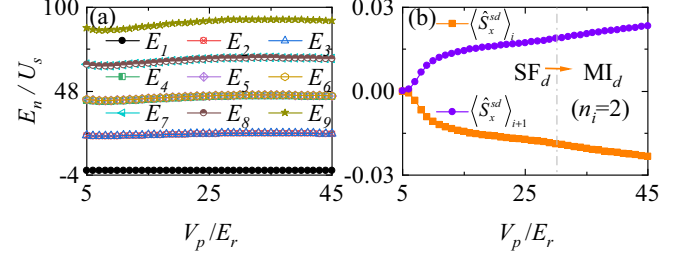


FIG. 7. (a) Eigenvalues E_n of the two-site model for perfect reflection $\eta = 1$. (b) Long-range orders for $n_i = 2$ under the ground state $|g_1\rangle$, calculated by using the parameters obtained via band-structure simulations. Other parameters are $N_{\text{lat}} \times U_0 = 600E_r$, $\Delta_c = 80\omega_r$, $\kappa = 40\omega_r$, and $\mu_s/U_s = 0.8$.

changes the eigenenergies but does not influence the orbital-density wave order.

B. Orbital-density wave order for filling $n_i = 2$ and reflection $\eta = 1$

We now extend the discussion to the case of two atoms per site with $n_i = 2$ in the deep Mott-insulating phase. In the basis of $|ss, ss\rangle$, $|ss, sd\rangle$, $|ss, dd\rangle$, $|sd, ss\rangle$, $|sd, sd\rangle$, $|sd, dd\rangle$, $|dd, ss\rangle$, $|dd, sd\rangle$, and $|dd, dd\rangle$, the two-site Hamiltonian can be written in matrix form (see Sec. A 4). After diagonalizing the Hamiltonian, we obtain the eigenstates

$$\begin{aligned} |g_n\rangle = & \sum_{\sigma,\sigma',\sigma'',\sigma'''} B_{n,\sigma\sigma',\sigma''\sigma'''} |\sigma\sigma', \sigma''\sigma'''\rangle \\ = & B_{n,ss,ss} |ss, ss\rangle + B_{n,ss,sd} |ss, sd\rangle + B_{n,ss,dd} |ss, dd\rangle \\ & + B_{n,sd,ss} |sd, ss\rangle + B_{n,sd,sd} |sd, sd\rangle + B_{n,sd,dd} |sd, dd\rangle \\ & + B_{n,dd,ss} |dd, ss\rangle + B_{n,dd,sd} |dd, sd\rangle \\ & + B_{n,dd,dd} |dd, dd\rangle, \end{aligned}$$

with eigenvalues E_n for $n = 1, 2, \dots, 8, 9$ and $J_1 = 2\text{Re}[\alpha] J_{sd}^{ii}$. Here, the states are defined as $|\sigma\sigma', \sigma''\sigma'''\rangle = \hat{b}_{i,\sigma}^\dagger \hat{b}_{i,\sigma'}^\dagger \hat{b}_{i+1,\sigma''}^\dagger \hat{b}_{i+1,\sigma'''}^\dagger |0, 0\rangle$. For the nondegenerate ground state $|g_1\rangle$ [shown Fig. 7(a)], we also obtain $\langle \hat{S}_x^{sd} \rangle_i = -\langle \hat{S}_x^{sd} \rangle_{i+1}$ in the d -orbital Mott-insulating phase, as shown in Fig. 7(b).

C. Orbital-density wave order for filling $n_i = 1$ and reflection $\eta < 1$

For an imperfect reflection of the pump laser, the field in the pump direction is not an ideal standing wave and possesses some running-wave component. In this case, the s -orbital atoms can be excited to both the p - and d -orbital states. In the absence of nearest-neighbor hopping terms, the Hamiltonian is given by

$$\begin{aligned} \hat{H}_0 = & - \sum_{i,\sigma} \mu_\sigma \hat{b}_{i,\sigma}^\dagger \hat{b}_{i,\sigma} + 2\text{Re}[\alpha] \\ & \times \sum_i (-1)^i (J_{sd}^{ii} \hat{b}_{i,s}^\dagger \hat{b}_{i,d} + J_{p_x p_y}^{ii} \hat{b}_{i,p_x}^\dagger \hat{b}_{i,p_y} + \text{H.c.}) \\ & + 2\text{Im}[\alpha] \sum_i (-1)^i (J_{s p_x}^{ii} \hat{b}_{i,s}^\dagger \hat{b}_{i,p_x} + J_{p_y d}^{ii} \hat{b}_{i,p_y}^\dagger \hat{b}_{i,d} + \text{H.c.}) \end{aligned}$$

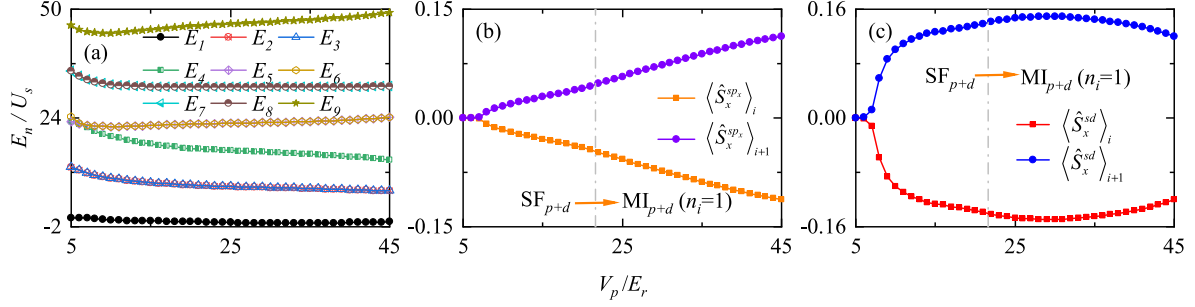


FIG. 8. (a) Eigenvalues E_n of the two-site model for imperfect reflection $\eta = 0.8$. (b) Long-range orders for the s orbital and p_x orbital with $n_i = 1$, calculated by using the real parameters obtained via band-structure simulations. (c) Long-range orders for the s orbital and d orbital. Other parameters are $N_{\text{lat}} \times U_0 = 1200E_r$, $\Delta_c = 100\omega_r$, $\kappa = 40\omega_r$, and $\mu_s/U_s = 0$.

$$+ \frac{1}{2} \sum_{i,\sigma,\sigma',\sigma'',\sigma'''} U_{\sigma\sigma'\sigma''\sigma'''} \hat{b}_{i,\sigma}^\dagger \hat{b}_{i,\sigma'}^\dagger \hat{b}_{i,\sigma''} \hat{b}_{i,\sigma'''}.$$

Without loss of generality, we focus on the case with filling $n_i = 1$ in the deep Mott-insulating phase. In the basis of $|s, s\rangle$, $|s, p_x\rangle$, $|s, d\rangle$, $|p_x, s\rangle$, $|p_x, p_x\rangle$, $|p_x, d\rangle$, $|d, s\rangle$, $|d, p_x\rangle$, and $|d, d\rangle$ the two-site Hamiltonian can be written in matrix form (see Sec. A 4).

After diagonalizing the Hamiltonian, the eigenstates are given by

$$\begin{aligned} |g_n\rangle &= \sum_{\sigma,\sigma'} C_{n;\sigma,\sigma'} |\sigma, \sigma'\rangle \\ &= C_{n;s,s} |s, s\rangle + C_{n;s,p_x} |s, p_x\rangle + C_{n;s,d} |s, d\rangle + C_{n;p_x,s} |p_x, s\rangle \\ &\quad + C_{n;p_x,p_x} |p_x, p_x\rangle + C_{n;p_x,d} |p_x, d\rangle + C_{n;d,s} |d, s\rangle \\ &\quad + C_{n;d,p_x} |d, p_x\rangle + C_{n;d,d} |d, d\rangle, \end{aligned}$$

with eigenenergies E_n for $n = 1, 2, \dots, 8, 9$, as shown in Fig. 8(a). The long-range orders under the ground state $|g_1\rangle$ are given by $\langle \hat{S}_x^{sp_x} \rangle_i = -\langle \hat{S}_x^{sp_x} \rangle_{i+1}$ and $\langle \hat{S}_x^{sd} \rangle_i = -\langle \hat{S}_x^{sd} \rangle_{i+1}$, as shown in Figs. 8(b) and 8(c).

V. EXPERIMENTAL DETECTIONS

For a perfect reflection of the pump laser, only s - and d -orbital atoms exist in the self-organized phase; the band-mapping techniques [18,68–70] can be used to distinguish atoms in different bands since the atoms mainly populate in the quasimomentum state $\mathbf{k} = (0, 0)$ for the s -orbital state and in $\mathbf{k} = (\pi, \pi)$ for the d -orbital one. But for the imperfect reflection, both the p - and d -orbital atoms mainly populate at the same point, $\mathbf{k} = (\pi, \pi)$. In this case, the population in higher-orbital bands can be measured from the images by nonadiabatically switching off the lattice [21,71,72].

VI. CONCLUSIONS

We study strongly interacting ultracold bosonic gases coupled to a high-finesse optical cavity pumped by a blue-detuned laser in the transverse direction. In contrast to the red-detuned case, we find that atoms can be excited into higher-orbital bands and self-organize into stable higher-orbital superfluid and Mott-insulating phases. By controlling the reflection of the pump laser, we find that atoms can be selectively pumped to the p - or d -orbital band of a two-dimensional square lattice,

providing different mechanics for controlling higher-orbital many-body phenomena. Our current setup involves only the square lattice and a single-mode cavity. Further work can be extended to complex lattice structures and multiple-cavity modes, where orbital frustrations come into play, inducing even richer many-body orbital phenomena.

ACKNOWLEDGMENTS

This work is supported by the National Natural Science Foundation of China under Grants No. 12074431, No. 11304386, and No. 11774428, Excellent Youth Foundation of Hunan Scientific Committee under Grant No. 2021JJ10044, and NSAF Grant No. U1930403. J.H. is supported by the Postgraduate Scientific Research Innovation Project of Hunan Province under Grant No. CX20200012. We acknowledge the Beijing Super Cloud Computing Center (BSCC) for providing HPC resources that contributed to the research results reported within this paper.

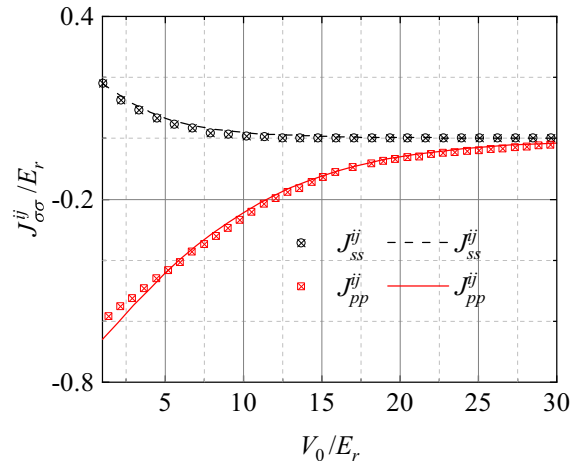


FIG. 9. Nearest-neighbor hopping amplitudes of J_{ss}^{ij} and J_{pp}^{ij} as a function of the lattice depth $V_0 \equiv V_x = V_y = V_z$, where the points, denoted by crosses, are from Ref. [66].

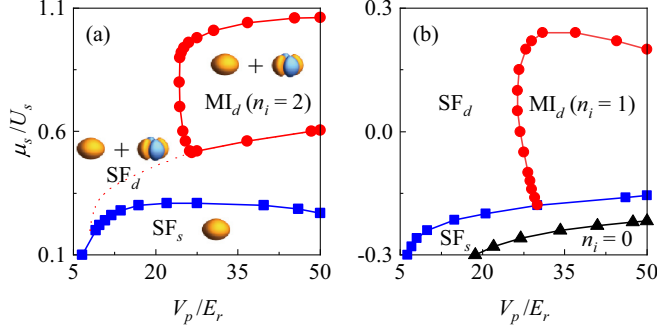


FIG. 10. Phase diagram of ultracold bosonic gases trapped in a cavity, pumped by a blue-detuned laser with the imbalance parameter $\eta = 1$ for different atom-cavity couplings (a) $N_{\text{lat}} \times U_0 = 500E_r$ and (b) $1200E_r$, obtained from bosonic dynamical mean-field theory. Here, there are three many-body phases, including the s -orbital superfluid phase (SF_s) in the absence of photons in the cavity, the d -orbital superfluid phase (SF_d) in the presence of photons in the cavity, and the d -orbital Mott-insulating phase (MI_d) with localized d -orbital atoms. Other parameters are $\Delta_c = 80\omega_r$ and $\kappa = 40\omega_r$.

APPENDIX

1. Extended Bose-Hubbard model

Following the standard procedures, the Hamiltonian

$$\begin{aligned} \hat{H} = & \int d\mathbf{x} \hat{\Psi}^\dagger(\mathbf{x}) \left(-\frac{\hbar^2}{2m} \nabla^2 + \eta V_p \sin^2(k_p y) \right. \\ & \left. + U_0 \sin^2(k_c x) \hat{a}^\dagger \hat{a} + \hat{V}_{1,\text{scat}} + \hat{V}_{2,\text{scat}} \right) \hat{\Psi}(\mathbf{x}) \\ & + \frac{g}{2} \int d\mathbf{x} \hat{\Psi}^\dagger(\mathbf{x}) \hat{\Psi}^\dagger(\mathbf{x}) \hat{\Psi}(\mathbf{x}) \hat{\Psi}(\mathbf{x}) - \hbar \Delta_c \hat{a}^\dagger \hat{a}, \quad (\text{A1}) \end{aligned}$$

with $\hat{V}_{1,\text{scat}} = \frac{(1+\eta)}{2} \sqrt{V_p U_0} (\hat{a} + \hat{a}^\dagger) \sin(k_c x) \sin(k_p y)$ and $\hat{V}_{2,\text{scat}} = i \frac{(1-\eta)}{2} \sqrt{V_p U_0} (\hat{a} - \hat{a}^\dagger) \sin(k_c x) \cos(k_p y)$, can be rewritten in the Wannier basis to obtain an extended Bose-Hubbard model in sufficiently deep lattices. We expand the atomic field operator in the Wannier basis set $\hat{\Psi}(\mathbf{x}) = \sum_{i,\sigma} \hat{b}_{i,\sigma} w_\sigma(\mathbf{x} - \mathbf{x}_i)$, where $\hat{b}_{i,\sigma}$ ($\hat{b}_{i,\sigma}^\dagger$) is the annihilation (creation) operator for a Wannier state σ at site i and $w_\sigma(\mathbf{x} - \mathbf{x}_i)$ is the Wannier function centered at $\mathbf{x} = \mathbf{x}_i$

for the s -, p_x -, p_y -, and d_{xy} -orbital states. The Bose-Hubbard Hamiltonian with on-site interactions has the following form:

$$\begin{aligned} \hat{H} = & - \sum_{(ij),\sigma} J_{\sigma\sigma}^{ij} \hat{b}_{i,\sigma}^\dagger \hat{b}_{j,\sigma} - \sum_{i,\sigma} \mu_\sigma \hat{b}_{i,\sigma}^\dagger \hat{b}_{i,\sigma} - \hbar \Delta_c \hat{a}^\dagger \hat{a} \\ & + \sum_{i,\sigma_1\sigma_2\sigma_3\sigma_4} \frac{U_{\sigma_1\sigma_2\sigma_3\sigma_4}}{2} \hat{b}_{i,\sigma_1}^\dagger \hat{b}_{i,\sigma_2}^\dagger \hat{b}_{i,\sigma_3} \hat{b}_{i,\sigma_4} + \hat{V}_1 + \hat{V}_2, \quad (\text{A2}) \end{aligned}$$

where $\mu_\sigma \equiv J_{\sigma\sigma}^{ii}$ is the chemical potential and the coupling between the pump laser and cavity mode $\hat{V}_1 = (\hat{a} + \hat{a}^\dagger) \sum_{ij} (-1)^i (J_{sd}^{ij} \hat{b}_{i,s}^\dagger \hat{b}_{j,d} + J_{p_x p_y}^{ij} \hat{b}_{i,p_x}^\dagger \hat{b}_{j,p_y} + \text{H.c.})$ and $\hat{V}_2 = -i(\hat{a} - \hat{a}^\dagger) \sum_{ij} (-1)^i (J_{s p_x}^{ij} \hat{b}_{i,s}^\dagger \hat{b}_{j,p_x} + J_{p_y d}^{ij} \hat{b}_{i,p_y}^\dagger \hat{b}_{j,d} + \text{H.c.})$. Here, (i, j) represents the nearest-neighbor sites i and j , the coupling matrix elements are

$$J_{\sigma\sigma}^{ij} = - \int d\mathbf{x} w_\sigma^*(\mathbf{x} - \mathbf{x}_i) \left(-\frac{\hbar^2 \nabla^2}{2m} + V_{\text{lat}} \right) w_\sigma(\mathbf{x} - \mathbf{x}_j), \quad (\text{A3})$$

$$\begin{aligned} J_{sd}^{ij} = & \int d\mathbf{x} w_{d_{xy}}^*(\mathbf{x} - \mathbf{x}_i) \frac{\sqrt{V_p U_0} (1 + \eta)}{2} \\ & \times \sin(k_c x) \sin(k_p y) w_s(\mathbf{x} - \mathbf{x}_j), \quad (\text{A4}) \end{aligned}$$

$$\begin{aligned} J_{p_x p_y}^{ij} = & \int d\mathbf{x} w_{p_y}^*(\mathbf{x} - \mathbf{x}_i) \frac{\sqrt{V_p U_0} (1 + \eta)}{2} \\ & \times \sin(k_c x) \sin(k_p y) w_{p_x}(\mathbf{x} - \mathbf{x}_j), \quad (\text{A5}) \end{aligned}$$

$$\begin{aligned} J_{s p_x}^{ij} = & - \int d\mathbf{x} w_{p_x}^*(\mathbf{x} - \mathbf{x}_i) \frac{\sqrt{V_p U_0} (1 - \eta)}{2} \\ & \times \sin(k_c x) \cos(k_p y) w_s(\mathbf{x} - \mathbf{x}_j), \quad (\text{A6}) \end{aligned}$$

$$\begin{aligned} J_{p_y d}^{ij} = & - \int d\mathbf{x} w_{d_{xy}}^*(\mathbf{x} - \mathbf{x}_i) \frac{\sqrt{V_p U_0} (1 - \eta)}{2} \\ & \times \sin(k_c x) \cos(k_p y) w_{p_y}(\mathbf{x} - \mathbf{x}_j), \quad (\text{A7}) \end{aligned}$$

$$\begin{aligned} U_{\sigma_1\sigma_2\sigma_3\sigma_4} = & \int d\mathbf{x} w_{\sigma_1}^*(\mathbf{x} - \mathbf{x}_i) w_{\sigma_2}^*(\mathbf{x} - \mathbf{x}_i) \\ & \times \frac{4\pi \hbar^2 a_s}{m} w_{\sigma_3}(\mathbf{x} - \mathbf{x}_i) w_{\sigma_4}(\mathbf{x} - \mathbf{x}_i), \quad (\text{A8}) \end{aligned}$$

and the on-site interaction terms read

$$\begin{aligned} \sum_{i,\sigma_1\sigma_2\sigma_3\sigma_4} \frac{U_{\sigma_1\sigma_2\sigma_3\sigma_4}}{2} \hat{b}_{i,\sigma_1}^\dagger \hat{b}_{i,\sigma_2}^\dagger \hat{b}_{i,\sigma_3} \hat{b}_{i,\sigma_4} = & \sum_i \left(\sum_{\sigma_1 \neq \sigma_2 \neq \sigma_3 \neq \sigma_4} U_{i,\sigma_1\sigma_2\sigma_3\sigma_4} (\hat{b}_{i,\sigma_1}^\dagger \hat{b}_{i,\sigma_2}^\dagger \hat{b}_{i,\sigma_3} \hat{b}_{i,\sigma_4} + \text{H.c.}) + \sum_\sigma \frac{U_{i,\sigma}}{2} \hat{n}_{i,\sigma} (\hat{n}_{i,\sigma} - 1) \right. \\ & \left. + \sum_{\sigma_1 \neq \sigma_2} 2U_{i,\sigma_1\sigma_2} \hat{n}_{i,\sigma_1} \hat{n}_{i,\sigma_2} + \sum_{\sigma_1 \neq \sigma_2} \frac{U_{i,\sigma_1\sigma_2}}{2} (\hat{b}_{i,\sigma_1}^\dagger \hat{b}_{i,\sigma_1}^\dagger \hat{b}_{i,\sigma_2} \hat{b}_{i,\sigma_2} + \text{H.c.}) \right), \quad (\text{A9}) \end{aligned}$$

where $V_{\text{lat}} = \eta V_p \sin^2(k_p y)$ in the pump direction and $V_{\text{lat}} = (V_{\text{cl}} + U_0 \hat{a}^\dagger \hat{a}) \sin^2(k_c x)$ in the cavity direction, with V_{cl} being an external optical lattice added in the cavity direction to validate the tight-binding model.

In order to simplify the effective Hamiltonian, we take the coherent-state approximation and represent the cavity mode by a complex amplitude α . In this case, the system depends on only the average photon number and is given by

$$\begin{aligned} \hat{H} = & - \sum_{(ij),\sigma} J_{\sigma\sigma}^{ij} (\hat{b}_{i,\sigma}^\dagger \hat{b}_{j,\sigma} + \text{H.c.}) + \sum_{i,\sigma_1\sigma_2\sigma_3\sigma_4} \frac{U_{\sigma_1\sigma_2\sigma_3\sigma_4}}{2} \hat{b}_{i,\sigma_1}^\dagger \hat{b}_{i,\sigma_2}^\dagger \hat{b}_{i,\sigma_3} \hat{b}_{i,\sigma_4} - \sum_{i,\sigma} \mu_\sigma \hat{b}_{i,\sigma}^\dagger \hat{b}_{i,\sigma} - \hbar |\alpha|^2 \Delta_c + 2\text{Re}[\alpha] \\ & \times \sum_{ij} (-1)^i (J_{sd}^{ij} \hat{b}_{i,s}^\dagger \hat{b}_{j,d} + J_{p_x p_y}^{ij} \hat{b}_{i,p_x}^\dagger \hat{b}_{j,p_y} + \text{H.c.}) + 2\text{Im}[\alpha] \sum_{ij} (-1)^i (J_{s p_x}^{ij} \hat{b}_{i,s}^\dagger \hat{b}_{j,p_x} + J_{p_y d}^{ij} \hat{b}_{i,p_y}^\dagger \hat{b}_{j,d} + \text{H.c.}), \quad (\text{A10}) \end{aligned}$$

where

$$\alpha = \frac{\sum_i (-1)^i \left(J_{sd}^{ii} \hat{b}_{i,s}^\dagger \hat{b}_{i,d} + J_{p_x p_y}^{ii} \hat{b}_{i,p_x}^\dagger \hat{b}_{i,p_y} + \text{H.c.} + i \left(J_{s p_x}^{ii} \hat{b}_{i,s}^\dagger \hat{b}_{i,p_x} + J_{p_y d}^{ii} \hat{b}_{i,p_y}^\dagger \hat{b}_{i,d} + \text{H.c.} \right) \right)}{\Delta_c - \sum_{i,\sigma} \langle J_\sigma \hat{b}_{i,\sigma}^\dagger \hat{b}_{i,\sigma} \rangle + i\kappa},$$

with $J_\sigma = \int d\mathbf{x} w_\sigma^*(\mathbf{x} - \mathbf{x}_i) U_0 \sin^2(k\mathbf{x}) w_\sigma(\mathbf{x} - \mathbf{x}_i)$ and κ being the decay rate of the cavity mode. We remark here that all the Hubbard parameters are obtained from the band-structure simulations, where the nearest-neighbor-hopping amplitudes for the lowest two bands are compared with the data from Ref. [66], as shown in Fig. 9. Actually, in a deep optical lattice, the localized wave functions can be described as the product of two Wannier functions for each direction, $w_s(\mathbf{x} - \mathbf{x}_i) = w_s(x)w_s(y)$, $w_{p_x}(\mathbf{x} - \mathbf{x}_i) = w_p(x)w_s(y)$, $w_{p_y}(\mathbf{x} - \mathbf{x}_i) = w_s(x)w_p(y)$, and $w_{d_y}(\mathbf{x} - \mathbf{x}_i) = w_p(x)w_p(y)$, where $w_s(x)$ and $w_p(x)$ [$w_s(y)$ and $w_p(y)$] denote the Wannier functions of the two lowest Bloch bands of a one-dimensional lattice in the x (y) direction.

2. Bosonic dynamical mean-field theory

a. BDMFT equations

We derive a self-consistent equation within bosonic dynamical mean-field theory (BDMFT) by using the cavity method [73], which is suitable for the high- but finite-dimensional optical lattice. The effective action of the impurity site up to subleading order in $1/z$ is described in the standard way [58,73]:

$$\begin{aligned} S_{\text{imp}}^{(0)} = & \int_0^\beta d\tau d\tau' \sum_{\sigma_1, \sigma'_1, \sigma_2, \sigma'_2} \begin{pmatrix} b_{0,\sigma_1}^*(\tau) \\ b_{0,\sigma_1}(\tau) \end{pmatrix}^T \mathcal{G}_{0,\sigma_1\sigma_2\sigma'_1\sigma'_2}^{-1}(\tau - \tau') \begin{pmatrix} b_{0,\sigma_2}(\tau') \\ b_{0,\sigma_2}^*(\tau') \end{pmatrix} - \int_0^\beta d\tau \sum_{\langle 0j \rangle, \sigma_1, \sigma'_1} (-1)^{\delta_{\sigma_1\sigma'_1}+1} J_{\sigma_1\sigma'_1}^{0j} [b_{0,\sigma_1}^*(\tau) \phi_{j,\sigma'_1}(\tau) + \text{H.c.}] \\ & + \int_0^\beta d\tau \left(\sum_{\sigma_1, \sigma'_1} J_{\sigma_1\sigma'_1}^{00} b_{0,\sigma_1}^*(\tau) b_{0,\sigma'_1}(\tau) + \text{H.c.} + \frac{1}{2} \sum_{\sigma_1\sigma_2\sigma_3\sigma_4} U_{\sigma_1\sigma_2\sigma_3\sigma_4} b_{\sigma_1}^{(0)*}(\tau) b_{\sigma_2}^{(0)*}(\tau) b_{\sigma_3}^{(0)}(\tau) b_{\sigma_4}^{(0)}(\tau) \right). \end{aligned} \quad (\text{A11})$$

To shorten the effective action, $J_{\sigma_1\sigma'_1}^{00}$ denotes the on-site scattering induced by the cavity mode and pump laser, and $J_{\sigma_1\sigma'_1}^{0j}$ are the nearest-neighbor hopping terms induced by the kinetic energy and the pump-cavity scattering. The Weiss Green's function (8×8 matrix) is defined as

$$\begin{aligned} & \mathcal{G}_{0,\sigma_1\sigma_2\sigma'_1\sigma'_2}^{-1}(\tau - \tau') \\ & = \begin{pmatrix} (\partial_\tau - \mu_{\sigma_1})\delta_{\sigma_1\sigma_2} + \sum_{\langle 0j \rangle, \langle 0j' \rangle} J_{\sigma_1\sigma'_1}^{0j} J_{\sigma_2\sigma'_2}^{0j'} G_{j,j',\sigma'_1,\sigma'_2}^1(\tau, \tau') & \sum_{\langle 0j \rangle, \langle 0j' \rangle} J_{\sigma_1\sigma'_1}^{0j} J_{\sigma_2\sigma'_2}^{0j'} G_{j,j',\sigma'_1,\sigma'_2}^2(\tau, \tau') \\ \sum_{\langle 0j \rangle, \langle 0j' \rangle} J_{\sigma_1\sigma'_1}^{0j} J_{\sigma_2\sigma'_2}^{0j'} G_{j,j',\sigma'_1,\sigma'_2}^{*2}(\tau', \tau) & (-\partial_{\tau'} - \mu_{\sigma_1})\delta_{\sigma_1\sigma_2} + \sum_{\langle 0j \rangle, \langle 0j' \rangle} J_{\sigma_1\sigma'_1}^{0j} J_{\sigma_2\sigma'_2}^{0j'} G_{j,j',\sigma'_1,\sigma'_2}^1(\tau', \tau) \end{pmatrix}, \end{aligned} \quad (\text{A12})$$

and we introduce

$$\phi_{j,\sigma_1}(\tau) \equiv \langle b_{j,\sigma_1}(\tau) \rangle_0 \quad (\text{A13})$$

as the superfluid order parameters and

$$G_{j,j',\sigma'_1,\sigma'_2}^1(\tau, \tau') = \langle b_{j,\sigma'_1}(\tau) b_{j',\sigma'_2}^*(\tau') \rangle_{(0)} - \phi_{j,\sigma'_1}(\tau) \phi_{j',\sigma'_2}^*(\tau'), \quad (\text{A14})$$

$$G_{j,j',\sigma'_1,\sigma'_2}^2(\tau, \tau') = \langle b_{j,\sigma'_1}(\tau) b_{j',\sigma'_2}(\tau') \rangle_{(0)} - \phi_{j,\sigma'_1}(\tau) \phi_{j',\sigma'_2}(\tau') \quad (\text{A15})$$

as the diagonal and off-diagonal parts of the connected Green's functions, respectively. Here, $\langle \dots \rangle_0$ takes the expectation value in the cavity system excluding the impurity site.

b. Anderson impurity model

It is difficult to find a solver analytically for the effective action (A11). Therefore, we return to the Hamiltonian representation to obtain BDMFT equations. The effective action (A11) can be represented by the Anderson impurity Hamiltonian

$$\begin{aligned} \hat{H}_A^{(0)} = & - \sum_{\sigma} J_{\sigma\sigma}^{0j} \left[\left(\phi_{\sigma}^{(0)*} \hat{b}_{\sigma}^{(0)} + \text{H.c.} \right) - \mu_{\sigma} \hat{n}_{\sigma}^{(0)} \right] + \frac{1}{2} \sum_{\sigma_1\sigma_2\sigma_3\sigma_4} U_{\sigma_1\sigma_2\sigma_3\sigma_4} b_{\sigma_1}^{(0)*}(\tau) b_{\sigma_2}^{(0)*}(\tau) b_{\sigma_3}^{(0)}(\tau) b_{\sigma_4}^{(0)}(\tau) \\ & + 2\text{Re}[\alpha] \left(J_{sd}^{0j} \hat{b}_s^{(0)*} \phi_d^{(0)} + J_{p_x p_y}^{0j} \hat{b}_{p_x}^{(0)*} \phi_{p_y}^{(0)} + \text{H.c.} \right) + 2\text{Im}[\alpha] \left(J_{s p_x}^{0j} \hat{b}_s^{(0)*} \phi_{p_x}^{(0)} + J_{p_y d}^{0j} \hat{b}_{p_y}^{(0)*} \phi_d^{(0)} + \text{H.c.} \right) \end{aligned}$$

$$\begin{aligned}
& + 2\text{Re}[\alpha](J_{sd}^{00}\hat{b}_s^{(0)*}\hat{b}_d^{(0)} + J_{p_x p_y}^{00}\hat{b}_{p_x}^{(0)*}\hat{b}_{p_y}^{(0)} + \text{H.c.}) + 2\text{Im}[\alpha](J_{s p_x}^{00}\hat{b}_s^{(0)*}\hat{b}_{p_x}^{(0)} + J_{p_y d}^{00}\hat{b}_{p_y}^{(0)*}\hat{b}_d^{(0)} + \text{H.c.}) \\
& + \sum_l \epsilon_l \hat{a}_l^\dagger \hat{a}_l + \sum_{l,\sigma} (V_{\sigma,l} \hat{a}_l^\dagger \hat{b}_\sigma^{(0)} + W_{\sigma,l} \hat{a}_l \hat{b}_\sigma^{(0)} + \text{H.c.}), \tag{A16}
\end{aligned}$$

where the on-site terms including the chemical potential, interaction, and on-site scattering terms are directly inherited from the Hubbard Hamiltonian. BDMFT couples two different baths, where the condensed bath of bosons is represented by the Gutzwiller term with superfluid order parameters $\phi_\sigma^{(0)}$ for the s -, p_x -, p_y -, and d_{xy} -orbital states. The normal bath of bosons is described by a finite number of orbitals with creation operators \hat{a}_l^\dagger and energies ϵ_l , where these orbitals are coupled to the impurity via normal-hopping amplitudes $V_{\sigma,l}$ and anomalous-hopping amplitudes $W_{\sigma,l}$, which are needed to generate the off-diagonal elements of the hybridization functions.

To obtain the solution of the impurity model, the Anderson Hamiltonian is straightforwardly implemented in the Fock basis, and the corresponding solution can be achieved by exact diagonalization of dynamical mean-field theory [59,73].

3. Phase diagrams for different Hubbard parameters with $\eta = 1$

We remark here that there is an intermediate parameter regime for the coupling $N_{\text{lat}} \times U_0$ where the scattering processes become pronounced, in contrast to the red-detuned case with larger coupling favoring self-organization of atoms. For a system with a perfect reflection with $\eta = 1$, we observe various interesting phases in the blue-detuned system which are stable for a large range of parameters. For example, we show the d -orbital superfluid and Mott-insulating phases for fillings $n_i = 1$ and 2 in Fig. 2. In this section, we discuss these phases in different parameter regimes. As shown in Figs. 10(a) and 10(b), there are also three many-body phases, including the s -orbital superfluid phase (SF_s) in the absence of photons in the cavity, the d -orbital superfluid phase (SF_d) in the presence of photons in the cavity, and the d -orbital Mott-insulating phase (MI_d) with localized d -orbital atoms.

4. The two-site Hamiltonian

a. Filling $n_i = 2$ and reflection $\eta = 1$

In the basis of $|ss, ss\rangle, |ss, sd\rangle, |ss, dd\rangle, |sd, ss\rangle, |sd, sd\rangle, |sd, dd\rangle, |dd, ss\rangle, |dd, sd\rangle$, and $|dd, dd\rangle$ the two-site Hamiltonian

$$\begin{aligned}
\hat{H}_0 = & 2\text{Re}[\alpha] \sum_i (-1)^i J_{sd}^{ii} (\hat{b}_{i,s}^\dagger \hat{b}_{i,d} + \text{H.c.}) + \frac{U_s}{2} \sum_i \hat{n}_{i,s} (\hat{n}_{i,s} - 1) + \frac{U_d}{2} \sum_i \hat{n}_{i,d} (\hat{n}_{i,d} - 1) + 2U_{sd} \hat{n}_{i,s} \hat{n}_{i,d} \\
& + \frac{U_{sd}}{2} (\hat{b}_{i,s}^\dagger \hat{b}_{i,s}^\dagger \hat{b}_{i,d} \hat{b}_{i,d} + \text{H.c.}) - \sum_{i,\sigma} \mu_\sigma \hat{b}_{i,\sigma}^\dagger \hat{b}_{i,\sigma} \tag{A17}
\end{aligned}$$

can be written as

$$H_0 = \begin{pmatrix} H_{0,(1,1)} & -J_1 & U_{sd} & J_1 & 0 & 0 & U_{sd} & 0 & 0 \\ -J_1 & H_{0,(2,2)} & -J_1 & 0 & J_1 & 0 & 0 & U_{sd} & 0 \\ U_{sd} & -J_1 & H_{0,(3,3)} & 0 & 0 & J_1 & 0 & 0 & U_{sd} \\ J_1 & 0 & 0 & H_{0,(4,4)} & -J_1 & U_{sd} & J_1 & 0 & 0 \\ 0 & J_1 & 0 & -J_1 & H_{0,(5,5)} & -J_1 & 0 & J_1 & 0 \\ 0 & 0 & J_1 & U_{sd} & -J_1 & H_{0,(6,6)} & 0 & 0 & J_1 \\ U_{sd} & 0 & 0 & J_1 & 0 & 0 & H_{0,(7,7)} & -J_1 & U_{sd} \\ 0 & U_{sd} & 0 & 0 & J_1 & 0 & -J_1 & H_{0,(8,8)} & -J_1 \\ 0 & 0 & U_{sd} & 0 & 0 & J_1 & U_{sd} & -J_1 & H_{0,(9,9)} \end{pmatrix}, \tag{A18}$$

with $J_1 = 2\text{Re}[\alpha]J_{sd}^{ii}$ and $H_{0,(1,1)} = -4\mu_s + 2U_s$, $H_{0,(2,2)} = -3\mu_s - \mu_d + U_s + 2U_{sd}$, $H_{0,(3,3)} = -2\mu_s - 2\mu_d + U_s + U_d$, $H_{0,(4,4)} = -3\mu_s - \mu_d + U_s + 2U_{sd}$, $H_{0,(5,5)} = -2\mu_s - 2\mu_d + 4U_{sd}$, $H_{0,(6,6)} = -\mu_s - 3\mu_d + U_d + 2U_{sd}$, $H_{0,(7,7)} = -2\mu_s - 2\mu_d + U_s + U_d$, $H_{0,(8,8)} = -\mu_s - 3\mu_d + U_d + 2U_{sd}$, and $H_{0,(9,9)} = -4\mu_d + 2U_d$.

b. Filling $n_i = 1$ and reflection $\eta < 1$

In the basis of $|s, s\rangle, |s, p_x\rangle, |s, d\rangle, |p_x, s\rangle, |p_x, p_x\rangle, |p_x, d\rangle, |d, s\rangle, |d, p_x\rangle$, and $|d, d\rangle$ the two-site Hamiltonian

$$\begin{aligned}
\hat{H}_0 = & 2\text{Re}[\alpha] \sum_i (-1)^i (J_{sd}^{ii} \hat{b}_{i,s}^\dagger \hat{b}_{i,d} + J_{p_x p_y}^{ii} \hat{b}_{i,p_x}^\dagger \hat{b}_{i,p_y} + \text{H.c.}) + 2\text{Im}[\alpha] \sum_i (-1)^i (J_{s p_x}^{ii} \hat{b}_{i,s}^\dagger \hat{b}_{i,p_x} + J_{p_y d}^{ii} \hat{b}_{i,p_y}^\dagger \hat{b}_{i,d} + \text{H.c.}) \\
& + \frac{1}{2} \sum_{i,\sigma,\sigma',\sigma'',\sigma'''} U_{\sigma\sigma'\sigma''\sigma'''} \hat{b}_{i,\sigma}^\dagger \hat{b}_{i,\sigma'}^\dagger \hat{b}_{i,\sigma''} \hat{b}_{i,\sigma'''} - \sum_{i,\sigma} \mu_\sigma \hat{b}_{i,\sigma}^\dagger \hat{b}_{i,\sigma} \tag{A19}
\end{aligned}$$

can be written as

$$H_0 = \begin{pmatrix} -2\mu_s & -J_2 & -J_1 & J_2 & 0 & 0 & J_1 & 0 & 0 \\ -J_2 & -\mu_s - \mu_{p_x} & 0 & 0 & J_2 & 0 & 0 & J_1 & 0 \\ -J_1 & 0 & -\mu_s - \mu_d & 0 & 0 & J_2 & 0 & 0 & J_1 \\ J_2 & 0 & 0 & -\mu_s - \mu_{p_x} & -J_2 & -J_1 & 0 & 0 & 0 \\ 0 & J_2 & 0 & -J_2 & -2\mu_{p_x} & 0 & 0 & 0 & 0 \\ 0 & 0 & J_2 & -J_1 & 0 & -\mu_{p_x} - \mu_d & 0 & 0 & 0 \\ J_1 & 0 & 0 & 0 & 0 & 0 & -\mu_s - \mu_d & -J_2 & -J_1 \\ 0 & J_1 & 0 & 0 & 0 & 0 & -J_2 & -\mu_{p_x} - \mu_d & 0 \\ 0 & 0 & J_1 & 0 & 0 & 0 & -J_1 & 0 & -2\mu_d \end{pmatrix}, \quad (\text{A20})$$

where $J_1 = 2\text{Re}[\alpha]J_{sd}^{ii}$ and $J_2 = 2\text{Im}[\alpha]J_{sp_x}^{ii}$.

-
- [1] L. de' Medici, S. R. Hassan, M. Capone, and X. Dai, *Phys. Rev. Lett.* **102**, 126401 (2009).
- [2] S. Kittaka, Y. Aoki, Y. Shimura, T. Sakakibara, S. Seiro, C. Geibel, F. Steglich, H. Ikeda, and K. Machida, *Phys. Rev. Lett.* **112**, 067002 (2014).
- [3] I. Bloch, *Nat. Phys.* **1**, 23 (2005).
- [4] Y. Tokura and N. Nagaosa, *Science* **288**, 462 (2000).
- [5] M. Lewenstein, A. Sanpera, V. Ahufinger, B. Damski, A. Sen, and U. Sen, *Adv. Phys.* **56**, 243 (2007).
- [6] I. Bloch, J. Dalibard, and W. Zwerger, *Rev. Mod. Phys.* **80**, 885 (2008).
- [7] T. Esslinger, *Annu. Rev. Condens. Matter Phys.* **1**, 129 (2010).
- [8] C. Wu, *Mod. Phys. Lett. B* **23**, 1 (2009).
- [9] O. Dutta, M. Gajda, P. Hauke, M. Lewenstein, D.-S. Lühmann, B. A. Malomed, T. Sowiński, and J. Zakrzewski, *Rep. Prog. Phys.* **78**, 066001 (2015).
- [10] X. Li and W. V. Liu, *Rep. Prog. Phys.* **79**, 116401 (2016).
- [11] A. Eckardt, *Rev. Mod. Phys.* **89**, 011004 (2017).
- [12] M. Bukov, L. D'Alessio, and A. Polkovnikov, *Adv. Phys.* **64**, 139 (2015).
- [13] G. Wirth, M. Ölschläger, and A. Hemmerich, *Nat. Phys.* **7**, 147 (2011).
- [14] M. Ölschläger, G. Wirth, and A. Hemmerich, *Phys. Rev. Lett.* **106**, 015302 (2011).
- [15] T. Kock, M. Ölschläger, A. Ewerbeck, W.-M. Huang, L. Mathey, and A. Hemmerich, *Phys. Rev. Lett.* **114**, 115301 (2015).
- [16] S. Jin, W. Zhang, X. Guo, X. Chen, X. Zhou, and X. Li, *Phys. Rev. Lett.* **126**, 035301 (2021).
- [17] X.-Q. Wang, G.-Q. Luo, J.-Y. Liu, W. V. Liu, A. Hemmerich, and Z.-F. Xu, *Nature (London)* **596**, 227 (2021).
- [18] T. Müller, S. Fölling, A. Widera, and I. Bloch, *Phys. Rev. Lett.* **99**, 200405 (2007).
- [19] S. Will, T. Best, U. Schneider, L. Hackermüller, D.-S. Lühmann, and I. Bloch, *Nature (London)* **465**, 197 (2010).
- [20] P. Soltan-Panahi, D.-S. Lühmann, J. Struck, P. Windpassinger, and K. Sengstock, *Nat. Phys.* **8**, 71 (2012).
- [21] Y. Zhai, X. Yue, Y. Wu, X. Chen, P. Zhang, and X. Zhou, *Phys. Rev. A* **87**, 063638 (2013).
- [22] L. Niu, S. Jin, X. Chen, X. Li, and X. Zhou, *Phys. Rev. Lett.* **121**, 265301 (2018).
- [23] J. Vargas, M. Nuske, R. Eichberger, C. Hippler, L. Mathey, and A. Hemmerich, *Phys. Rev. Lett.* **126**, 200402 (2021).
- [24] M. Hachmann, Y. Kiefer, J. Riebesehl, R. Eichberger, and A. Hemmerich, *Phys. Rev. Lett.* **127**, 033201 (2021).
- [25] H. Ritsch, P. Domokos, F. Brennecke, and T. Esslinger, *Rev. Mod. Phys.* **85**, 553 (2013).
- [26] F. Mivehvar, F. Piazza, T. Donner, and H. Ritsch, *Adv. Phys.* **70**, 1 (2021).
- [27] P. Domokos and H. Ritsch, *Phys. Rev. Lett.* **89**, 253003 (2002).
- [28] D. E. Chang, J. I. Cirac, and H. J. Kimble, *Phys. Rev. Lett.* **110**, 113606 (2013).
- [29] T. Griebner and H. Ritsch, *Phys. Rev. Lett.* **111**, 055702 (2013).
- [30] J. Keeling, M. J. Bhaseen, and B. D. Simons, *Phys. Rev. Lett.* **112**, 143002 (2014).
- [31] F. Piazza and P. Strack, *Phys. Rev. Lett.* **112**, 143003 (2014).
- [32] Y. Chen, Z. Yu, and H. Zhai, *Phys. Rev. Lett.* **112**, 143004 (2014).
- [33] G. R. M. Robb, E. Tesio, G.-L. Oppo, W. J. Firth, T. Ackemann, and R. Bonifacio, *Phys. Rev. Lett.* **114**, 173903 (2015).
- [34] Y. Li, L. He, and W. Hofstetter, *Phys. Rev. A* **87**, 051604(R) (2013).
- [35] M. R. Bakhtiari, A. Hemmerich, H. Ritsch, and M. Thorwart, *Phys. Rev. Lett.* **114**, 123601 (2015).
- [36] K. Baumann, C. Guerlin, F. Brennecke, and T. Esslinger, *Nature (London)* **464**, 1301 (2010).
- [37] H. Keßler, J. Klinder, M. Wolke, and A. Hemmerich, *Phys. Rev. Lett.* **113**, 070404 (2014).
- [38] R. Landig, L. Hruby, N. Dogra, M. Landini, R. Mottl, T. Donner, and T. Esslinger, *Nature (London)* **532**, 476 (2016).
- [39] J. Klinder, H. Keßler, M. R. Bakhtiari, M. Thorwart, and A. Hemmerich, *Phys. Rev. Lett.* **115**, 230403 (2015).
- [40] M. Landini, N. Dogra, K. Kroeger, L. Hruby, T. Donner, and T. Esslinger, *Phys. Rev. Lett.* **120**, 223602 (2018).
- [41] R. M. Kroeze, Y. Guo, V. D. Vaidya, J. Keeling, and B. L. Lev, *Phys. Rev. Lett.* **121**, 163601 (2018).
- [42] M. A. Norcia, R. J. Lewis-Swan, and J. R. K. Cline, *Science* **361**, 259 (2018).
- [43] R. M. Kroeze, Y. Guo, and B. L. Lev, *Phys. Rev. Lett.* **123**, 160404 (2019).
- [44] J. Keeling, M. J. Bhaseen, and B. D. Simons, *Phys. Rev. Lett.* **105**, 043001 (2010).
- [45] N. Liu, J. Lian, J. Ma, L. Xiao, G. Chen, J. Q. Liang, and S. Jia, *Phys. Rev. A* **83**, 033601 (2011).
- [46] M. J. Bhaseen, J. Mayoh, B. D. Simons, and J. Keeling, *Phys. Rev. A* **85**, 013817 (2012).

- [47] F. Piazza and H. Ritsch, *Phys. Rev. Lett.* **115**, 163601 (2015).
- [48] F. Mivehvar, H. Ritsch, and F. Piazza, *Phys. Rev. Lett.* **118**, 073602 (2017).
- [49] H. Keßler, J. G. Cosme, M. Hemmerling, L. Mathey, and A. Hemmerich, *Phys. Rev. A* **99**, 053605 (2019).
- [50] H. Keßler, J. G. Cosme, C. Georges, L. Mathey, and A. Hemmerich, *New J. Phys.* **22**, 085002 (2020).
- [51] R. Lin, P. Mognini, A. U. J. Lode, and R. Chitra, *Phys. Rev. A* **101**, 061602(R) (2020).
- [52] N. Masalaeva, W. Niedenzu, F. Mivehvar, and H. Ritsch, *Phys. Rev. Research* **3**, 013173 (2021).
- [53] P. Zupancic, D. Dreon, X. Li, A. Baumgärtner, A. Morales, W. Zheng, N. R. Cooper, T. Esslinger, and T. Donner, *Phys. Rev. Lett.* **123**, 233601 (2019).
- [54] X. Li, D. Dreon, P. Zupancic, A. Baumgärtner, A. Morales, W. Zheng, N. R. Cooper, T. Donner, and T. Esslinger, *Phys. Rev. Research* **3**, L012024 (2021).
- [55] C. Maschler and H. Ritsch, *Phys. Rev. Lett.* **95**, 260401 (2005).
- [56] J. Larson, B. Damski, G. Morigi, and M. Lewenstein, *Phys. Rev. Lett.* **100**, 050401 (2008).
- [57] K. Baumann, R. Mottl, F. Brennecke, and T. Esslinger, *Phys. Rev. Lett.* **107**, 140402 (2011).
- [58] K. Byczuk and D. Vollhardt, *Phys. Rev. B* **77**, 235106 (2008).
- [59] A. Hubener, M. Snoek, and W. Hofstetter, *Phys. Rev. B* **80**, 245109 (2009).
- [60] P. Anders, E. Gull, L. Pollet, M. Troyer, and P. Werner, *Phys. Rev. Lett.* **105**, 096402 (2010).
- [61] Y. Li, M. R. Bakhtiari, L. He, and W. Hofstetter, *Phys. Rev. B* **84**, 144411 (2011).
- [62] B. Capogrosso-Sansone, N. V. Prokof'ev, and B. V. Svistunov, *Phys. Rev. B* **75**, 134302 (2007).
- [63] Y. Li, J. Yuan, A. Hemmerich, and X. Li, *Phys. Rev. Lett.* **121**, 093401 (2018).
- [64] K. R. A. Hazzard and E. J. Mueller, *Phys. Rev. A* **81**, 031602(R) (2010).
- [65] O. Dutta, A. Eckardt, P. Hauke, B. Malomed, and M. Lewenstein, *New J. Phys.* **13**, 023019 (2011).
- [66] D.-S. Lühmann, O. Jürgensen, and K. Sengstock, *New J. Phys.* **14**, 033021 (2012).
- [67] U. Bissbort, F. Deuretzbacher, and W. Hofstetter, *Phys. Rev. A* **86**, 023617 (2012).
- [68] A. Kastberg, W. D. Phillips, S. L. Rolston, R. J. C. Spreeuw, and P. S. Jessen, *Phys. Rev. Lett.* **74**, 1542 (1995).
- [69] M. Greiner, I. Bloch, O. Mandel, T. W. Hänsch, and T. Esslinger, *Phys. Rev. Lett.* **87**, 160405 (2001).
- [70] M. Köhl, H. Moritz, T. Stöferle, K. Günter, and T. Esslinger, *Phys. Rev. Lett.* **94**, 080403 (2005).
- [71] D. Hu, L. Niu, B. Yang, X. Chen, B. Wu, H. Xiong, and X. Zhou, *Phys. Rev. A* **92**, 043614 (2015).
- [72] X. Zhou, S. Jin, and J. Schmiedmayer, *New J. Phys.* **20**, 055005 (2018).
- [73] A. Georges, G. Kotliar, W. Krauth, and M. J. Rozenberg, *Rev. Mod. Phys.* **68**, 13 (1996).